Global DGLAP fit analyses of the nPDF: EKS98 and HKM*

K.J. Eskola[a,b], *H. Honkanen*[a,b], *V.J. Kolhinen*[a], *C.A. Salgado*[c]
[a]*Department of Physics, P.O. Box 35, FIN-40014 University of Jyväskylä, Finland*
[b]*Helsinki Institute of Physics, P.O. Box 64, FIN-00014 University of Helsinki, Finland,*
[c]*CERN, Theory Division, CH-1211 Geneva, Switzerland*

Abstract
The DGLAP analyses of the nuclear parton distribution functions (nPDF) based on the global fits to the data are reviewed, and the results from EKS98 and HKM are compared. The usefulness of measuring hard probes in pA collisions, at the LHC in particular, is demonstrated.

1. Introduction

Inclusive cross sections for hard processes $A+B \to c+X$ involving a sufficiently large scale $Q \gg \Lambda_{\rm QCD}$ are computable by using collinear factorization. In the leading twist approximation power corrections $\sim 1/Q^2$ are neglected and

$$d\sigma(Q^2,\sqrt{s})_{AB\to c+X} = \sum_{i,j=q,\bar{q},g} \left[Z_A f_i^{p/A}(x_1,Q^2) + (A-Z_A) f_i^{n/A}(x_1,Q^2) \right] \otimes$$
$$\otimes \left[Z_B f_j^{p/B}(x_2,Q^2) + (B-Z_B) f_j^{n/B}(x_2,Q^2) \right] \otimes d\hat{\sigma}(Q^2,x_1,x_2)_{ij\to c+x} \qquad (1)$$

where A, B are the colliding hadrons or nuclei containing Z_A and Z_B protons correspondingly, c the produced parton, x and X anything, $d\hat{\sigma}(Q^2,x_1,x_2)_{ij\to c+x}$ the perturbatively calculable differential cross section for the production of c at the scale Q, and $x_{1,2} \sim Q/\sqrt{s}$ the fractional momenta of the colliding partons i and j. The number distribution function of the parton flavour i of the protons (neutrons) in A is denoted as $f_i^{p/A}$ ($f_i^{n/A}$), and similarly for partons j in B.

In the leading twist approximation multiple scattering of the bound nucleons does occur but all collisions are independent, correlations between partons from the same object A are neglected, and only one-parton densities are needed. The parton distribution functions (PDF) $f_i^{p/A}$ are universal quantities and applicable in all collinearly factorizable processes. The PDF cannot be computed by perturbative methods, and so far it has not been possible to compute them from first principles, either. Thus, nonperturbative input from data on various hard processes is needed for the extraction of the PDF. However, once the PDF are known at some initial (lowest) scale $Q_0 \gg \Lambda_{\rm QCD}$, the QCD perturbation theory predicts the scale evolution of the PDF to other (higher) values of Q^2 in form of the Dokshitzer-Gribov-Lipatov-Altarelli-Parisi (DGLAP) equations [1].

The method to extract the PDF from experimental data is well established in the case of the free proton: the initial (non-perturbative) distributions are parametrized at some Q_0^2, and evolved to higher scales according to the DGLAP equations. Comparison with the data is made at various regions of the (x,Q^2)-plane, and the parameters of the initial distributions $f_i^p(x,Q_0^2)$ become fixed when the best global fit is found. The data from deeply inelastic lp scattering (DIS) are of main importance in these global DGLAP fits, especially the HERA data at small values of x and Q^2. The sum rules for momentum, charge and baryon number give further constraints. In this way, through the global DGLAP fits, groups like MRST [2], CTEQ [3] or GRV [4] obtain their well-known sets of the PDF of the free proton.

*Contribution to CERN Yellow Report on Hard Probes in Heavy Ion Collisions at the LHC.

The nuclear parton distribution functions (nPDF) differ in magnitude from the PDF of the free proton. In the measurements of the structure function $F_2^A = Z_A F_2^{p/A} + (A - Z_A)F_2^{n/A}$ of nuclear targets in DIS (see e.g. [5] for references) and especially of the ratio

$$R_{F_2}^A(x,Q^2) \equiv \frac{\frac{1}{A}d\sigma^{lA}/dQ^2dx}{\frac{1}{2}d\sigma^{lD}/dQ^2dx} \approx \frac{\frac{1}{A}F_2^A(x,Q^2)}{\frac{1}{2}F_2^D(x,Q^2)}, \tag{2}$$

the following nuclear effects have been discovered as a function of Bjorken-x:

- shadowing; a depletion $R_{F_2}^A < 1$ at $x \lesssim 0.1$,
- anti-shadowing; an excess $R_{F_2}^A > 1$ at $0.1 \lesssim x \lesssim 0.3$,
- EMC effect; a depletion at $0.3 \lesssim x \lesssim 0.7$, and
- Fermi motion; an excess towards $x \to 1$ and beyond.

The Q^2 dependence of $R_{F_2}^A$ is weaker and has thus been more difficult to measure. Data with high enough precision, however, exist: NMC has some years ago discovered a clear Q^2 dependence in the ratio $d\sigma^{\mu\mathrm{Sn}}/d\sigma^{\mu\mathrm{C}}$ [6], i.e. the scale dependence of the ratio $F_2^{\mathrm{Sn}}/F_2^{\mathrm{C}}$, at $x \gtrsim 0.01$. Since $F_2^{p(n)/A} = \sum_q e_q^2 x[f_q^{p(n)/A} + f_{\bar{q}}^{p(n)/A}] + \mathcal{O}(\alpha_s)$, the nuclear effects in the ratio $R_{F_2}^A$ directly translate into nuclear effects in the parton distributions; $f_i^{p/A} \neq f_i^p$.

The nPDF $f_i^{p/A}$ also obey the DGLAP equations in the large-Q^2 limit, and they can be determined by using a similar global DGLAP fit procedure as in the case of the PDF of the free proton. Pioneering studies of the DGLAP evolution of the nPDF are e.g. [7, 8, 9, 10]. References for various other studies of perturbative evolution of the nPDF and also to simpler Q^2-independent parametrizations of the nuclear effects in the PDF can be found e.g. in [11, 12]. The nuclear case is, however, more complicated because of additional variables, the mass number A and the charge Z, and, because the number of data points available in the perturbative region is more limited than for the PDF of the free proton. The DIS data plays the dominant role in the nuclear case as well. However, as illustrated by Fig. 1, no data are available from nuclear DIS experiments below $x \lesssim 5 \cdot 10^{-3}$ at $Q^2 \gtrsim 1$ GeV^2. This makes the determination of the nuclear gluon distributions especially difficult. Further constraints for the global DGLAP fits of the nPDF can be obtained from e.g. the Drell-Yan (DY) process measured in fixed-target pA collisions [13, 14]. Currently, there are two sets of nPDF available which are based on the global DGLAP fits to the data: (i) EKS98 [15, 16] (the code in [17, 18]), and (ii) HKM [19] (the code in [20]). We shall compare the main features of these two analyses and comment on their differences below.

2. Comparison of EKS98 and HKM

2.1 EKS98 and overview of constraints available from data

The parametrization EKS98 prepared in [15] is based on the results of the DGLAP analysis in [16] and its follow-up in [15]. We shall here refer to these together as EKRS. In the EKRS approach the nPDF, the parton distributions of the bound *protons*, $f_i^{p/A}$, are defined through the modifications of the corresponding distributions in the free proton,

$$R_i^A(x,Q^2) \equiv \frac{f_i^{p/A}(x,Q^2)}{f_i^p(x,Q^2)}, \tag{3}$$

where the PDF of the free proton are from a known set, such as CTEQ, MRS or GRV. As in the case of the free nucleons, for isoscalar nuclei the parton distributions of bound neutrons are obtained through isospin symmetry, $f_{u(\bar{u})}^{n/A} = f_{d(\bar{d})}^{p/A}$ and $f_{d(\bar{d})}^{n/A} = f_{u(\bar{u})}^{p/A}$. Although exact only for isoscalar and mirror nuclei, this is expected to be a good first approximation for all nuclei.

To simplify the determination of the input nuclear effects for valence and sea quarks, the following flavour-independent *initial* modifications are assumed: $R_{u_V}^A(x,Q_0^2) \approx R_{d_V}^A(x,Q_0^2) \approx R_V^A(x,Q_0^2)$, and

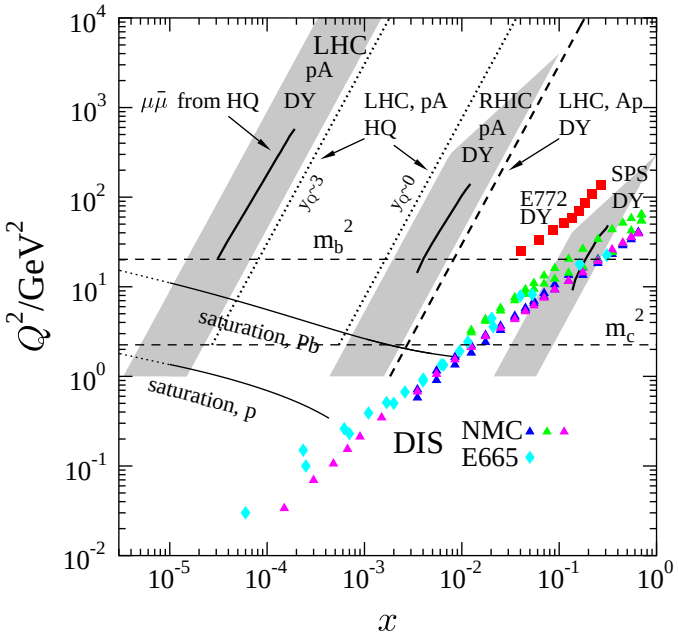

Fig. 1: The average values of x and Q^2 of the DIS data from NMC [21, 22, 23] (triangles) and E665 [24, 25] (diamonds) in lA, and of x_2 and M^2 of the DY dilepton data [13] (squares) in pA. The heavy quark mass scales are shown by the horizontal dashed lines. The initial scale Q_0^2 is m_c^2 in EKRS and 1 GeV^2 in HKM. The rest of the figure: see the text in Sec. 3.1.

$R_{\bar{u}}^A(x,Q_0^2) \approx R_{\bar{d}}^A(x,Q_0^2) \approx R_s^A(x,Q_0^2) \approx R_S(x,Q_0^2)$. Thus only three independent initial ratios, R_V^A, R_S^A and R_G^A are to be determined at $Q_0^2 = m_c^2 = 2.25$ GeV^2. Note also that the approximations above are needed and used *only* at Q_0^2 in [16]. In the EKS98-parametrization [15] of the DGLAP-evolved results, it was observed that to a good approximation $R_{u_V}^A = R_{d_V}^A$ and $R_{\bar{u}}^A = R_{\bar{d}}^A$ for all Q^2. Further details of the EKRS analysis can be found in [16], here we summarize the constraints available in each region of x. Consider first quarks and antiquarks:

- At $x \gtrsim 0.3$ the DIS data constrains only the ratio R_V^A: valence quarks dominate F_2^A, so $R_{F_2}^A \approx R_V^A$ but R_S^A and R_G^A are left practically unconstrained. An EMC effect is, however, assumed also for the initial R_S^A and R_G^A since in the scale evolution the EMC effect of valence quarks is transmitted to gluons and further on to sea quarks [9]. In this way the nuclear modifications R_i^A also remain stable against the evolution.
- At $0.04 \lesssim x \lesssim 0.3$ both the DIS and DY data constrain R_S^A and R_V^A but from different regions of Q^2, as shown in Fig. 1. In addition, conservation of baryon number restricts R_V^A. The use of DY data [13] is essential in order to fix the relative magnitude of R_V^A and R_S^A, since the DIS data alone cannot distinguish between them. As a result, no antishadowing appears in $R_S^A(x,Q_0^2)$.
- At $5 \cdot 10^{-3} \lesssim x \lesssim 0.04$ only DIS data exist in the region $Q \gtrsim 1$ GeV where the DGLAP analysis can be expected to apply. Once R_V^A is fixed by the DIS and DY data at larger x, the magnitude of nuclear valence quark shadowing in the EKRS approach follows from the conservation of baryon number. As a result of these contraints, nuclear valence quarks in EKRS are less shadowed than the sea quarks, $R_V^A > R_S^A$.
- At $x \lesssim 5 \cdot 10^{-3}$, as shown by Fig. 1, the DIS data for the ratio $R_{F_2}^A$ lie in the region $Q \lesssim 1$ GeV where the DGLAP equations are unlikely to be applicable in the nuclear case. Indirect constraints, however, *can* be obtained by noticing: (i) At the smallest values of x (where $Q \ll 1$ GeV), $R_{F_2}^A$ depends only very weakly, if at all, on x [22, 24]. (ii) $\partial(F_2^{\rm Sn}/F_2^{\rm C})/\partial \log Q^2 > 0$ at $x \sim 0.01$ [6], indicating that $\partial R_{F_2^A}/\partial \log Q^2 > 0$. (iii) Negative $\log Q^2$-slopes of $R_{F_2}^A$ at $x \lesssim 5 \cdot 10^{-3}$ have not

been observed [22]. Based on these experimental facts, it is assumed in the EKRS approach that the sign of the $\log Q^2$-slope of $R^A_{F_2}$ remains non-negative at $x < 0.01$ and therefore the DIS data [22, 24] in the non-perturbative region gives a *lower bound* for $R^A_{F_2}$ at Q^2_0 at very small x. The sea quarks dominate over the valence quarks at small values of x, so only R^A_S becomes constrained by the DIS data; R^A_V remains restricted by baryon number conservation.

Pinning down the nuclear gluon distributions is difficult in the absense of stringent direct constraints. What is available in different regions of x can be summarized as follows:

- At $x \gtrsim 0.2$ no experimental constraints are currently available for the gluons. Conservation of momentum is used as an overall constraint but this alone is not sufficient to determine whether an EMC effect exists for gluons or not: only about 30 % of the gluon momentum comes from $x \gtrsim 0.2$, so fairly sizable changes in $R^A_G(x, Q^2_0)$ in this region can be compensated by smaller changes at $x < 0.2$ without violating the constraints discussed below. As mentioned above, in the EKRS approach an EMC effect is initially assumed for R_G. This guarantees a stable scale evolution; the EMC effect remains there also at larger Q^2.
- At $0.02 \lesssim x \lesssim 0.2$ the Q^2 dependence of the ratio $F_2^{\rm Sn}/F_2^{\rm C}$ measured by NMC [6] sets the currently most important constraint for R^A_G, as first pointed out in [26]. In the small-x region where gluons dominate the DGLAP evolution, the Q^2 dependence of $F_2(x, Q^2)$ is dictated by the gluon distribution as [27] $\partial F_2(x, Q^2)/\partial \log Q^2 \sim \alpha_s x g(2x, Q^2)$. This leads to [16, 11] $\partial R^A_{F_2}(x, Q^2)/\partial \log Q^2 \sim \alpha_s [R^A_G(2x, Q^2) - R^A_{F_2}(x, Q^2)] x g(2x, Q^2)/F^D_2(x, Q^2)$. The $\log Q^2$ slopes of $F_2^{\rm Sn}/F_2^{\rm C}$ measured by NMC [6] therefore constrain R^A_G. Especially, as discussed in detail in [16, 11], the positive $\log Q^2$-slope of $F_2^{\rm Sn}/F_2^{\rm C}$ measured by NMC indicates that $R^A_G(2x, Q^2_0) > R^A_{F_2}(x, Q^2_0)$ at $x \sim 0.01$. Thus, within the DGLAP framework, a gluon shadowing at $x \sim 0.01$ which would be much stronger than the shadowing of antiquarks, such as suggested e.g. in [28], is not supported by the NMC data. The antishadowing in the EKRS gluons follows from the constraint $R^A_G(0.03, Q^2_0) \approx 1$ imposed by the NMC data (see also [26]) combined with the requirement of momentum conservation. The EKRS antishadowing is consistent with the E789 data [29] on D-meson production in pA collisions (notice, however, the large error bar of the data point), and it seems to be supported by the J/Ψ production in DIS, measured by NMC [30].
- At $x \lesssim 0.02$, stringent experimental constraints do not exist for the nuclear gluons at the moment. It should be emphasized, however, that the initial R^A_G in this region is directly connected with the initial $R^A_{F_2}$. As discussed above, related to quarks at small x, taking the DIS data on $R^A_{F_2}$ in the non-perturbative region as a lower limit for $R^A_{F_2}$ at Q^2_0 corresponds to $\partial R_{F_2^A}/\partial \log Q^2 \geq 0$, and thus $R^A_G(x < 0.02, Q^2_0) \geq R^A_{F_2}(x/2, Q^2_0) \geq R^A_{F_2}(x/2, Q^2 \ll 1\,{\rm GeV}^2)$. The observation in [16] was that setting $R^A_G(x, Q^2_0) \approx R^A_{F_2}(x, Q^2_0)$ at $x \lesssim 0.01$ fulfills this constraint. This approximation remains fairly good even after the DGLAP evolution from $Q_0 \sim 1$ GeV to $Q \sim 100$ GeV, see [15].

As explained in detail in [16], in the EKRS approach the initial ratios $R^A_V(x, Q^2_0)$, $R^A_S(x, Q^2_0)$ and $R^A_G(x, Q^2_0)$ are constructed piecewize in different regions of x. Initial nPDF are computed at Q^2_0, LO DGLAP evolution to higher scales is performed and comparison with DIS and DY data is made. The parameters in the input ratios are iteratively changed until the best global fit to the data is achieved. The determination of the input parameters in EKRS has so far been done only manually, the best overall fit is determined by eye. For the quality of the obtained fit, see the detailed comparison with the data in Figs. 4-10 of [16]. The parametrization EKS98 [15] of the nuclear modifications $R^A_i(x, Q^2)$ was prepared on the basis of the results in [16]. It was also shown that when the PDF of the free proton where changed from GRVLO [31] to CTEQ4L [32] (differing from each other considerably), the changes induced to $R^A_i(x, Q^2)$ were within a few percents [15]. Therefore, accepting this range of uncertainty, the EKS98 parametrization can be used together with any (LO) set of the PDF of the free proton.

2.2 The HKM analysis

In principle, the definition of the nPDF in the HKM analysis [19] differs slightly from that in EKRS: instead of the PDF of the bound protons, HKM define the nPDF as the *average* distributions of each flavour i in a nucleus A: $f_i^A(x,Q^2) = (Z/A)f_i^{p/A}(x,Q^2) + (1-Z/A)f_i^{n/A}(x,Q^2)$. Correspondingly, the HKM nuclear modifications at the initial scale $Q_0^2 = 1$ GeV^2 are then defined through

$$f_i^A(x,Q_0^2) = w_i(x,A,Z)[(Z/A)f_i^p(x,Q_0^2) + (1-Z/A)f_i^n(x,Q_0^2)]. \quad (4)$$

In practice, however, since in the EKS98 parametrization one sets $R_{u_V}^A = R_{d_V}^A$ and $R_{\bar{u}}^A = R_{\bar{d}}^A$, also the EKS98 modifications represent average modifications. Flavour-symmetric sea quark distributions are assumed in HKM, whereas the flavour asymmetry of the sea quarks in EKRS follows from that of the free proton.

An improvement relative to EKRS is that the HKM method to extract the initial modifications $w_i(x,A,Z)$ at Q_0^2 is more automatic and more quantitative in the statistical analysis; the HKM analysis is strictly a minimum-χ^2 fit. Also, with certain assumptions of a suitable form (see [19]) for the initial modifications w_i, the number of parameters has been brought conveniently down to seven. The form used is

$$w_i(x,A,Z) = 1 + \left(1 - \frac{1}{A^{1/3}}\right)\frac{a_i(A,Z) + H_i(x)}{(1-x)^{\beta_i}}, \quad (5)$$

where $H_i(x) = b_i x + c_i x^2$ (analysis with a cubic polynomial is also performed, with similar results). Due to the flavour-symmetry, the sea quark parameters are identical for all flavours. For valence quarks, conservation of charge Z (not used in EKRS) and baryon number A are required; this fixes a_{u_V} and a_{d_V}. In the case of non-isoscalar nuclei $w_{u_V} \neq w_{d_V}$. Also momentum conservation is imposed; this fixes a_g. Taking β_V, b_V, c_V to be the same for u_V and d_V, and $\beta_{\bar{q}} = \beta_g = 1$, $b_g = -2c_g$, the remaining seven parameters b_V, c_V, β_V, $a_{\bar{q}}$ $b_{\bar{q}}$, $c_{\bar{q}}$, c_g are determined by a global DGLAP fit which minimizes the χ^2.

2.3 The comparison

Irrespective of whether the best fit is found automatically or by eye, the basic procedure to determine the nPDF in the EKRS and HKM analyses is the same. The results obtained for the nuclear effects are, however, quite different, as can be seen in the comparison at $Q^2 = 2.25$ GeV^2 shown in Fig. 2. The main reason for this is that different data sets are used:

- The HKM analysis [19] uses only the DIS data, whereas EKRS include also the DY data from pA collisions. As explained above, the DY data is very important in the EKRS analysis in fixing the relative modifications of valence and sea quarks at intermediate x. Preliminary results reported in [33] show that when the DY data is included in the HKM analysis, the antiquark modifications will become more similar to those in EKRS.
- The NMC data set on $F_2^A/F_2^{\rm C}$ [23], which imposes quite stringent constraints for the A-systematics in the EKRS analysis, is not used in HKM. As a result, $R_{F_2}^A$ has less shadowing in HKM than in EKRS (see also Fig. 1 of [11]), especially for heavy nuclei.
- In addition to the recent DIS data sets, some older ones are used in the HKM analysis. The older sets are not included in EKRS. This, however, is presumably not causing any major differences between EKRS and HKM, since the older data come with larger errorbars, and are therefore typically of less statistical weight in the χ^2 analysis.
- The HKM analysis does not make use of the NMC data [6] on the Q^2 dependence of $F_2^{\rm Sn}/F_2^{\rm C}$. As explained above, these data are the main experimental constraint for the nuclear gluons in the EKRS analysis. Fig. 3 shows a comparison between the EKRS (solid), the HKM (dotted-dashed) results and the NMC data on $F_2^{\rm Sn}/F_2^{\rm C}$ as a function of Q^2. As observed there, the HKM results do not reproduce the measured Q^2 dependence of $F_2^{\rm Sn}/F_2^{\rm C}$ at the smallest values of x. This figure demonstrates explicitly that the nuclear modifications of gluon distributions at $0.02 \lesssim x \lesssim 0.1$ *can* be pinned down with help of these NMC data.

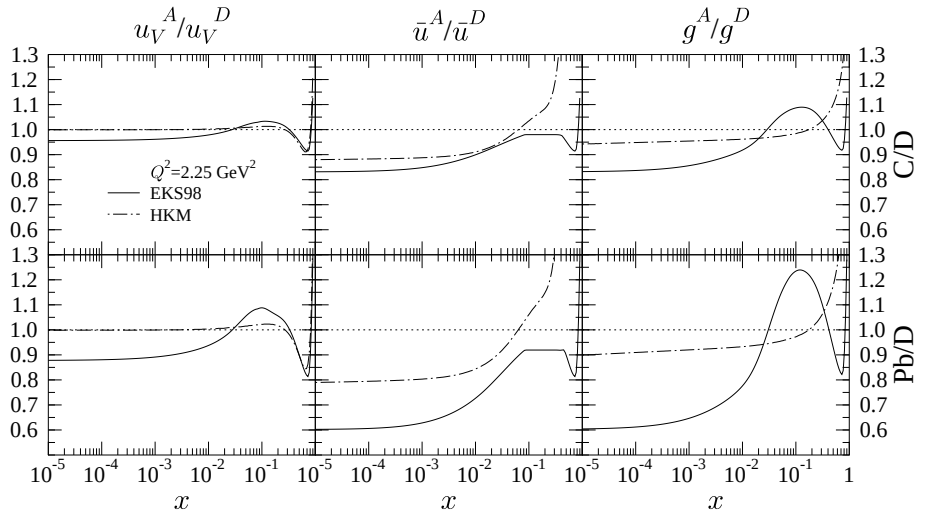

Fig. 2: The nuclear modifications for the u_V, $\bar{u}$ and gluon distributions in EKS98 (solid) and in HKM (dotted dashed) at $Q^2 = 2.25$ GeV^2. Upper panels: C/D. Lower panels: Pb/D, with isoscalar Pb.

3. Future prospects

3.1 Constraints from pA collisions at LHC, RHIC and SPS

The hard probes in pA collisions, especially those in LHC, will play a major role in probing the nPDF at regions not accessed before. This is sketched in Fig. 1, showing the regions in x and Q^2 probed by certain hard processes at different cms-energies. Let us consider the figure in more detail:

• The measurements of semileptonic decays of D and $\bar{D}$ mesons in pA will help in pinning down the nuclear gluon distributions [34, 35]. Borrowed from a LO analysis [35], the thick solid lines in Fig. 1 show how the average scale $Q^2 = \langle m_T^2 \rangle$ of open charm production is correlated with the average fractional momentum $x = \langle x_2 \rangle$ of the incoming nuclear gluon in dimuon production from correlated $D\bar{D}$ pairs at the LHC (computed for pPb at $\sqrt{s} = 5500$ GeV, $2.5 \leq y_\mu \leq 4.0$, with no rapidity shifts), at RHIC (pAu at $\sqrt{s} = 200$ GeV, $1.15 \leq y_\mu \leq 2.44$) and at the SPS ($p$Pb at $\sqrt{s} = 17.3$ GeV, $0 \leq y_\mu \leq 1$). For each solid curve, the smallest Q^2 shown corresponds to a dimuon invariant mass $M = 1.25$ GeV, and the the largest Q^2 to $M = 9.5$ GeV (LHC), 5.8 GeV (RHIC) and 4.75 GeV (SPS) (cf. Fig. 5 in [35]). We observe that data from the SPS, RHIC and LHC will offer constraints in different regions of x: the data from NA60 in the SPS will probe the antishadowing of nuclear gluons and the RHIC data the beginning of the gluon shadowing, while the LHC data will constrain the nuclear gluons at very small x, deep in the shadowing region.

• Similarly, the DY cross sections of dimuons in pA are expected to set more constraints on the nuclear effects of sea quark distributions. In $2 \to 2$ kinematics $x_2 = (M/\sqrt{s})e^{-y}$, where M and y are the invariant mass and rapidity of the lepton pair. The rapidity of the pair is always between the rapidities of the leptons forming the pair. The shaded regions in Fig. 1 illustrate the regions in $x = x_2^A$ and $Q^2 = M^2$ probed by the DY dimuons in pA collisions at the LHC, RHIC and SPS. The parameters used for the LHC are $\sqrt{s} = 5500$ GeV, $2.5 \leq y \leq 4.0$ with no rapidity shifts [36]. Note that from the point of view of x_2^A (but *not* of x_1^p), Pb+Pb collisions at $\sqrt{s}_{\rm PbPb} = 5500$ GeV at the LHC are equivalent to pPb collisions at $\sqrt{s}_{p\rm Pb} = 8800$ GeV: the decrease of x_2 due to the increase in $\sqrt{s}$ is compensated by an increase from the rapidity shift y_0 [36]: $x_2^{pA} = (M/\sqrt{s}_{pA})e^{-(y_{AA}+y_0)} = (M/\sqrt{s}_{AA})e^{-y_{AA}} = x_2^{AA}$. For RHIC, the shaded region corresponds to $\sqrt{s} = 200$ GeV, and $1.2 \leq y \leq 2.2$, which is the rapidity acceptance region of the forward muon arm in PHENIX [37]. For the SPS, we have again used $\sqrt{s} = 17.3$ GeV and $0 \leq y \leq 1$. Single muon p_T-cuts (see [38, 37]) have not been applied, the shaded regions all correspond

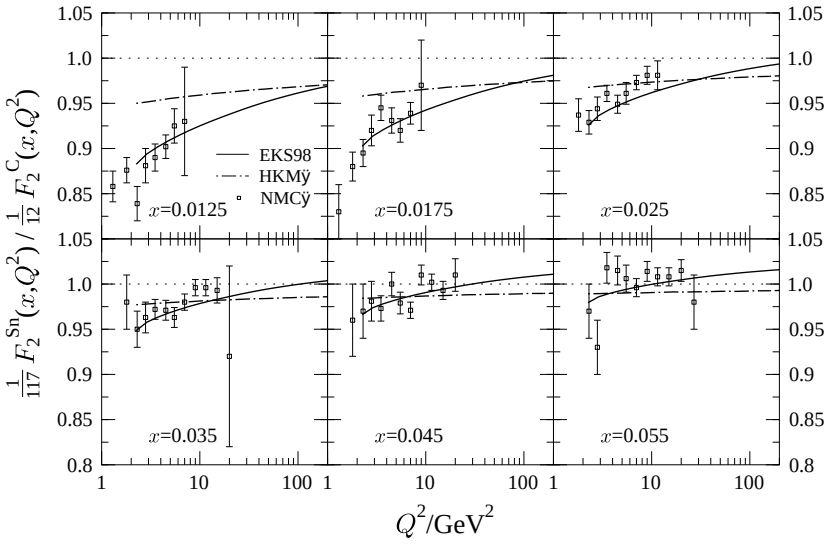

Fig. 3: The ratio $F_2^{\rm Sn}/F_2^{\rm C}$ as a function of Q^2 at different fixed values of x. The data is from NMC [6] and the curves are EKS98 [15] (solid) and HKM [19] (dotted dashed).

to $M^2 \geq 1$ GeV^2. At the highest scales shown, the dimuon regions at the SPS and RHIC are limited by the end of the phase space. The SPS data may shed more light on the question of an EMC effect for the sea quarks [39]. The DY dimuons at the LHC will probe the sea quark distributions deep in the shadowing region and also at high scales, especially also at $Q^2 = M_Z^2$. The region of RHIC data is again conveniently in between the SPS and LHC, mainly probing the beginning of the shadowing region of sea quarks. In Ap collisions at the LHC, the DY dimuons with $y = (y_{\rm min} + y_{\rm max})/2$ probe the regions plotted with the dashed line (the spread due to the y acceptance is not shown).

• The dotted line shows the kinematical region probed by open heavy quark production in pA (and also in AA), when both heavy quarks are at $y = 0$ in the ALICE detector frame. In this case again, assuming $2 \to 2$ kinematics, $x_2^{pA} = x_2^{AA} = 2m_T/\sqrt{s}_{AA}$. To illustrate the effect of moving towards forward rapidities, also the case $y_Q = y_{\overline{Q}} = 3$ is shown. Only the region at $Q^2 \gtrsim m_b^2$ (above the upper horizontal line) is probed by $b\bar{b}$ production. Due to the same kinematics as in open $Q\overline{Q}$ production, the dotted lines also correspond to the regions probed by direct photon production.

• As demonstrated by Fig. 1, the hard probes in pA collisions at RHIC and at the LHC in particular will provide us with very important constraints for the nPDF at scales where the DGLAP evolution can be expected to be applicable. Power corrections in the evolution [41, 42] can, however, be expected to play an increasingly important role towards small values of x and Q^2. The effects of the first of such corrections, the GLRMQ terms [41, 42] leading to nonlinear DGLAP+GLRMQ evolution equations, have been recently studied in [43] in light of the HERA data. From the point of view of the DGLAP evolution of the (n)PDF, saturation of gluons takes place when their evolution becomes dominated by the power corrections [40]. Fig. 1 shows the saturation limits obtained for the free proton and for Pb in the DGLAP+GLRMQ approach [44] (solid curves; the dotted extrapolations are merely for guiding the eye). The saturation limit obtained for the free proton in the DGLAP+GLRMQ analysis should be taken as an upper limit in Q^2 but it is constrained quite well by the HERA data (see [43]). In obtaining the saturation limit shown for the Pb nucleus in [44], the constraints from the Q^2 dependence of $F_2^{\rm Sn}/F_2^{\rm C}$, however, have not yet been taken into account. For a comparison of the saturation limits obtained in other models, see [44].

• Fig. 1 shows also which hard probes in pA collisions can be expected to probe the nPDF in the gluon saturation region. Especially the probes directly sensitive to the gluon distributions are

interesting from this point of view. Such probes would be open $c\bar{c}$ production at small p_T, and direct photon production at $p_T \sim$ few GeV, both at as forward rapidities as possible (see the dotted lines). Note that open $b\bar{b}$ production is already in the applicability region of the linear DGLAP evolution. In light of the saturation limits shown, the chances for measuring the effects of nonlinearities in the evolution through open $c\bar{c}$ production in pA at RHIC would seem marginal. At the LHC, however, measuring saturation effects in the nuclear gluon distributions through open $c\bar{c}$ in pA could be possible.

3.2 Improvements of the DGLAP analyses

On the practical side, the global DGLAP fit analyses of the nPDF discussed above can be improved in obvious ways. The EKRS analysis should be made more automatic and a proper statistical treatment, such as in HKM, should be added. The automatization alone is, however, not expected to change the nuclear modifications of the PDF significantly from EKS98 but more quantitative estimates of the uncertainties and of their propagation would be obtained. This work is in progress. As also discussed above, more data contraints should be added to the HKM analysis. More generally, all presently available data from hard processes in DIS and pA collisions have not yet been exhausted: for instance, the recent DIS data for $F_2^{\nu\mathrm{Fe}}$ and $F_3^{\nu\mathrm{Fe}}$ from νFe and $\bar{\nu}$Fe collisions by CCFR[45] (not used in EKRS or in HKM), could help in pinning down the valence quark modifications [46]. In the future, the hard probes in pA collisions at the LHC, RHIC and the SPS will offer very important constraints for the nPDF, especially for gluons and sea quarks. Eventually, the nPDF DGLAP analyses should be extended to NLO perturbative QCD. As discussed above, the effects of power corrections [41, 42] to the DGLAP equations and also to the cross sections [47] should be analysed in detail in context with the global fits to the nuclear data.

Acknowledgements. We thank N. Armesto, F. Gelis, P.V. Ruuskanen, I. Vitev and other participants of the CERN Hard Probes workshops for discussions. We are grateful for the Academy of Finland, Project 50338, for financial support. C.A.S. is supported by a Marie Curie Fellowship of the European Community programme TMR (Training and Mobility of Researchers), under the contract number HPMF-CT-2000-01025.

References

[1] Y. L. Dokshitzer, Sov. Phys. JETP **46** (1977) 641 [Zh. Eksp. Teor. Fiz. **73** (1977) 1216]; V. N. Gribov and L. N. Lipatov, Yad. Fiz. **15** (1972) 781, 1218 [Sov. J. Nucl. Phys. **15** (1972) 438, 675]; G. Altarelli and G. Parisi, Nucl. Phys. B **126** (1977) 298.

[2] A. D. Martin, R. G. Roberts, W. J. Stirling and R. S. Thorne, Eur. Phys. J. C **23** (2002) 73 [arXiv:hep-ph/0110215].

[3] J. Pumplin, D. R. Stump, J. Huston, H. L. Lai, P. Nadolsky and W. K. Tung, JHEP **0207** (2002) 012 [arXiv:hep-ph/0201195].

[4] M. Gluck, E. Reya and A. Vogt, Eur. Phys. J. C **5** (1998) 461 [arXiv:hep-ph/9806404].

[5] M. Arneodo, Phys. Rept. **240** (1994) 301.

[6] M. Arneodo *et al.* [New Muon Collaboration], Nucl. Phys. B **481** (1996) 23.

[7] J. w. Qiu, Nucl. Phys. B **291** (1987) 746.

[8] L. L. Frankfurt, M. I. Strikman and S. Liuti, Phys. Rev. Lett. **65** (1990) 1725.

[9] K. J. Eskola, Nucl. Phys. B **400** (1993) 240.

[10] S. Kumano, Phys. Rev. C **50** (1994) 1247 [arXiv:hep-ph/9402321]; S. Kumano and M. Miyama, Phys. Lett. B **378** (1996) 267 [arXiv:hep-ph/9512244].

[11] K. J. Eskola, H. Honkanen, V. J. Kolhinen and C. A. Salgado, Phys. Lett. B **532** (2002) 222 [arXiv:hep-ph/0201256].

[12] K. J. Eskola, H. Honkanen, V. J. Kolhinen, P. V. Ruuskanen and C. A. Salgado, arXiv:hep-ph/0110348.

[13] D. M. Alde *et al.*, Phys. Rev. Lett. **64** (1990) 2479.

[14] M. A. Vasilev *et al.* [FNAL E866 Collaboration], Phys. Rev. Lett. **83** (1999) 2304 [arXiv:hep-ex/9906010].

[15] K. J. Eskola, V. J. Kolhinen and C. A. Salgado, Eur. Phys. J. C **9** (1999) 61 [arXiv:hep-ph/9807297].

[16] K. J. Eskola, V. J. Kolhinen and P. V. Ruuskanen, Nucl. Phys. B **535** (1998) 351 [arXiv:hep-ph/9802350].

[17] http://urhic.phys.jyu.fi/; http://www-fp.usc.es/phenom/.

[18] H. Plothow-Besch, Int. J. Mod. Phys. A **10** (1995) 2901.

[19] M. Hirai, S. Kumano and M. Miyama, Phys. Rev. D **64** (2001) 034003 [arXiv:hep-ph/0103208].

[20] http://www-hs.phys.saga-u.ac.jp.

[21] P. Amaudruz *et al.* [New Muon Collaboration], Nucl. Phys. B **441** (1995) 3 [arXiv:hep-ph/9503291].

[22] M. Arneodo *et al.* [New Muon Collaboration.], Nucl. Phys. B **441** (1995) 12 [arXiv:hep-ex/9504002].

[23] M. Arneodo *et al.* [New Muon Collaboration], Nucl. Phys. B **481** (1996) 3.

[24] M. R. Adams *et al.* [E665 Collaboration], Phys. Rev. Lett. **68** (1992) 3266.

[25] M. R. Adams *et al.* [E665 Collaboration], Z. Phys. C **67** (1995) 403 [arXiv:hep-ex/9505006].

[26] T. Gousset and H. J. Pirner, Phys. Lett. B **375** (1996) 349 [arXiv:hep-ph/9601242].

[27] K. Prytz, Phys. Lett. B **311** (1993) 286.

[28] S. y. Li and X. N. Wang, Phys. Lett. B **527** (2002) 85 [arXiv:nucl-th/0110075].

[29] M. J. Leitch *et al.* [E789 Collaboration], Phys. Rev. Lett. **72** (1994) 2542.

[30] P. Amaudruz *et al.* [New Muon Collaboration], Nucl. Phys. B **371** (1992) 553.

[31] M. Gluck, E. Reya and A. Vogt, Z. Phys. C **53** (1992) 127.

[32] H. L. Lai *et al.*, Phys. Rev. D **55** (1997) 1280 [arXiv:hep-ph/9606399].

[33] S. Kumano, Nucl. Phys. Proc. Suppl. **112** (2002) 42 [arXiv:hep-ph/0204242].

[34] Z. w. Lin and M. Gyulassy, Phys. Rev. Lett. **77** (1996) 1222 [Heavy Ion Phys. **4** (1996) 123] [arXiv:nucl-th/9510041].

[35] K. J. Eskola, V. J. Kolhinen and R. Vogt, Nucl. Phys. A **696** (2001) 729 [arXiv:hep-ph/0104124].

[36] A. Morsch, in this CERN Yellow Report.

[37] J. L. Nagle [the PHENIX Collaboration], arXiv:nucl-ex/0209015.

[38] M. Botje, in this CERN Yellow Report.

[39] K. J. Eskola, V. J. Kolhinen, C. A. Salgado and R. L. Thews, Eur. Phys. J. C **21** (2001) 613 [arXiv:hep-ph/0009251].

[40] Jianwei Qiu, in this CERN Yellow Report.

[41] L. V. Gribov, E. M. Levin and M. G. Ryskin, Phys. Rept. **100** (1983) 1.

[42] A. H. Mueller and J. w. Qiu, Nucl. Phys. B **268** (1986) 427.

[43] K. J. Eskola, H. Honkanen, V. J. Kolhinen, J. w. Qiu and C. A. Salgado, arXiv:hep-ph/0211239.

[44] V. J. Kolhinen, in this CERN Yellow Report.

[45] W. G. Seligman *et al.*, Phys. Rev. Lett. **79** (1997) 1213.

[46] M. Botje, Eur. Phys. J. C **14** (2000) 285 [arXiv:hep-ph/9912439].

[47] X. f. Guo, J. w. Qiu and W. Zhu, Phys. Lett. B **523** (2001) 88 [arXiv:hep-ph/0110038].